Polymerization shrinkage of resin-based composites for dental restorations: A digital volume correlation study

Marta Gallo, Hazem Abouelleil, Jean Marc Chenal, Jérôme Adrien, Joël Lachambre, Pierre Colon, Éric Maire

Version of Record: https://www.sciencedirect.com/science/article/pii/S0109564119308486
Manuscript_ebb82656c8167ed88b16ebb83d9f1e10

Polymerization shrinkage of resin-based composites for dental restorations: a digital volume correlation study

Marta Gallo[a], Hazem Abouelleil[b], Jean Marc Chenal[a], Jérôme Adrien[a], Joël Lachambre[a], Pierre Colon[b,c], Eric Maire[a]

a Univ Lyon, INSA de Lyon, MATEIS UMR CNRS 5510, Bât. Saint Exupery, 23 Av. Jean Capelle, F-69621 Villeurbanne, France
b Laboratoire des Multimateriaux et Interfaces, UMR CNRS 5615, Universite Lyon1, Villeurbanne, France
c UFR d'odontologie, Université Paris Diderot, APHP, Hopital Rothschild, Service d'odontologie, Paris, France

Corresponding Author

Eric Maire, eric.maire@insa-lyon.fr, MATEIS Lab Batiment St Exupery 3rd floor, INSA de LYON, 69621 Villeurbanne cedex FRANCE

Abstract

Objectives

Resin-based composites are widely used in dental restorations; however, their volumetric shrinkage during polymerization leads to several issues that reduce the restoration survival rates. For overcoming this problem, a deep study of shrinkage phenomena is necessary.

Methods

In this study, micro-tomography (µ-CT) is combined with digital volume correlation (DVC) to investigate the effect of several factors on the polymerization strain of dental composites in model cavities: the presence/absence of an adhesive, the use of transparent/blackened cavities, and irradiation times between 1 and 40 s.

Results

The results indicate that the presence of an adhesive at the interface between the cavity and composite does not reduce the total strain but instead limits it to a preferential direction. In addition, regardless of the conditions, the main strain is generated along the axis parallel to the polymerization irradiation (the vertical axis). Finally, the total strain appears to occur in the first 5 s of irradiation, with no further evolution observed for longer irradiation times.

Significance

This work provides new insight into resin-based composite shrinkage and demonstrates the benefit of coupling DVC and µ-CT to better understand the degradation mechanisms of these materials.

Keywords: polymerization shrinkage, adhesion, micro-tomography, Digital Volume Correlation, strain, *in situ* tests

1. Introduction

Resin-based composites are widely used for dental restorations because of their similarity to natural teeth as well as their suitable mechanical properties. However, according to long-term studies on patients, degradation occurs at the margins of large restorations with survival times between 8 and 12 years [1–3]. One of the major disadvantages of current composites is their polymerization shrinkage, which is typically observed for dimethacrylate resins [4,5]. During the cross-linking process (induced by light irradiation), the polymer chains become more packed, causing a decrease in volume (2%–3% on average [6]). This polymerization shrinkage leads to the formation of inner stresses that can cause pain to the patient, strain at the margins, interfacial gaps, and microleakage, leading to secondary caries and eventually restoration failure [7,8].

Recently, several studies have been performed on the polymerization shrinkage of dental restorations. In the first studies, the leakage was assessed by immersing the sample in a dye, sectioning it, and then visually evaluating the dye penetration at the interface between the restoration and cavity. However, this technique is destructive and only provides qualitative (or semi-quantitative) results as it strongly depends on the degree of dye penetration and cannot be applied to the entire sample volume. To overcome these issues, Carrera *et al*. [8] suggested an approach involving the use of micro-tomography (µ-CT) (as reported in [9]). An initial µ-CT scan of the sample was performed followed by immersion of the specimen in a radio-opaque dye (silver nitrate solution) and a second µ-CT scan. The dye volume was isolated by subtraction of the first scan from the second scan. Although this method is non-destructive and more precise, it still relies on the penetration of the dye in the

interfacial gaps. Moreover, this approach can be complicated if the contrast between the dental material and tooth structure is limited, as demonstrated by Jacker-Guhr *et al.* [10].

Another technique for direct evaluation of the polymerization shrinkage rather than the leakage was proposed by Sun *et al.* [11,12]. The specimens were scanned using μ-CT (resolution of 18 μm) before and after polymerization, and the shrinkage was calculated by subtracting the first reconstructed volume from the second [11]. The results were coherent with those observed using dye penetration [12] (resolution of 16 μm).

Other studies have coupled μ-CT analyses with particle tracking to determine both the total shrinkage and the displacement vector field for the entire specimen volume. Experiments have been performed both with and without adhesive. Chiang *et al.* [13,14] applied this technique to human molars (scan resolution of 8 μm), and Cho *et al.* [15] applied it to both artificial model cavities and real teeth (scan resolution of 14.2 μm). In all cases, radiolucent particles (30-μm-diameter spherical zirconia [15], 40–90-μm-diameter spherical glass fillers [13,14]) were added to the composites for the particle tracking. The results of these studies differed, with shrinkage toward the center of the specimen observed in some works and shrinkage toward the light source or downward in the opposite direction observed in others. As suggested by Chiang *et al.* [14], the discrepancy between the results can be explained by the differences in adhesion between the composite and the wall of the cavity (enamel and dentin in natural teeth) and bottom of the cavity (pure dentin). Indeed, the composite is expected to shrink toward the interface with strongest adhesion (e.g., the interface with enamel in real teeth). In general, the addition of particles (e.g., zirconia or glass beads) as markers raises a concern because if the particles are not silanized, they may not have a strong enough connection to the composite [14]. Even if the particles are silanized, their presence will affect the viscosity of the resin composite as well as the shrinkage behavior [16]. To overcome these issues, Takemura *et al.* [16] suggested the use of air bubbles as markers. Although this technique appears to be simple and effective, bubbles are intentionally incorporated in the composite, whereas, dentists attempt to avoid the presence

of air bubbles; therefore, it is unclear whether this approach is representative of the clinical reality.

Moreover, the strain fields induced by shrinkage were not reported in any of these previous studies. This information is fundamental for assessing the residual stresses inside the material and thus inferring the possibility of failure of the dental restoration.

Contrarily to previous works, where deformations were assessed by the particle tracking technique [13–16], in the present study, we used µ-CT and digital volume correlation (DVC) with a global approach to measure the displacement field (and, by derivation, the strain field) during the shrinkage of dental resins. The studied composites contained large fillers in their microstructure, which were used as a natural contrast 'speckle' pattern [17] for the DVC measurement, similarly to the use of inclusions inherently present in metals [18] or solid foams [19]. Because of this, the addition of any supplementary filler, often reported in the literature [13–15], was not mandatory, excluding any possible influence of the additional filler on shrinkage behavior. This technique enabled us to evaluate the total strain of the composite and assess the displacement and deformation fields in the entire specimen volume. Conversely to previous works, the present study focuses not only on global shrinkage [11,12], mean deformation [13,14] or axial deformation [15], but also on deformations in the transversal plane (perpendicular to the irradiation direction) throughout the sample's height. Finally, as a further progress compared to the state of the art, µ-CT scans were acquired in our study with a resolution higher (4.5 µm) than that reported in previous studies (8-18 µm) and we also highlight the influence of a constraint on shrinkage.

The above-described procedure was applied to different cavity models (i.e., transparent/blackened) with or without the presence of an adhesive at the cavity/composite interface for various irradiation times. Our aim was to evaluate the evolution of polymerization shrinkage with time and the effect of the presence of the adhesive (i.e., in presence of a constraint).

2. Materials and Methods

To verify the influence of the experimental conditions on curing, some preliminary trials were made using the commercial product Clearfil Photo Core by Kuraray Noritake (Japan) (68 wt.% silica and barium glass particles). The composite was placed in a plastic straw (Φ 4 mm) in the µ-CT chamber and images were periodically acquired (every 7 seconds) in radiography mode (i.e., without rotating the specimen) with a resolution of 3.5 µm. For evaluating the influence of time, the uncured sample was covered with a lid, imaged, let in place for 3 hours and imaged again. Possible changes in the specimen can be revealed by subtracting the first image to the final one. For assessing the influence of the µ-CT chamber light, the same test was performed, but without any lid and for a longer time (16h). For checking the influence of X-Ray, the uncured sample was imaged continuously for 3 hours. Finally, samples were cured using a commercial blue-light LED curing unit (EliparTM DeepCureS, 3M ESPE) and imaged again.

Apart from the preliminary tests, the composite used for this study was supplied by DMG Chemisch-Pharmazeutische Fabrik (Hamburg, Germany). The composite consisted of 80 wt.% particles (79 wt.% of silanated barium glass particles with an average size of 7 µm and 1.1 wt.% of pyrogenic silica with an average size of 0.04 µm). The remaining 20 wt.% was a resin matrix composed of a mixture of Bis-phenol A-glycidyl methacrylate (Bis-GMA), urethane dimethacrylate (UDMA), triethyleneglycol dimethacrylate (TEGDMA), and ethoxylated bisphenol A dimethacrylate (EBPADMA). The experiments were performed using standardized cavities (4-mm diameter and 4-mm high) drilled in poly methyl methacrylate (PMMA) cubes. The outer surfaces of the cubes were either left as received or painted black with a permanent marker to hinder the path of light. In some tests, two incremental layers of adhesive (ScotchbondTM Universal, 3M ESPE) were applied to the walls of the cavity, and each layer was photo-polymerized for 15 s. Photo-polymerization of the adhesive and composite was induced using a commercial blue-light LED curing unit (EliparTM DeepCureS, 3M ESPE).

The polymerization shrinkage was assessed using in situ µ-CT analyses. The samples were scanned before irradiation, irradiated *in situ* in the sample holder, and then scanned again. The scans were performed using a laboratory tomograph with a voxel resolution of 4.5 µm following the procedure previously described by Buffiere *et al.* [20]. The X-ray tube was operated at 80 kV and 280 µA. For each scan, 900 images were acquired (without any filter) with an exposure time of 333 µs for each image, leading to a total scan duration of 20 min. The samples were scanned at different polymerization times up to 40 s, which is the irradiation time applied in dental practice. For the "interrupted" tests, a specimen without adhesive was scanned, irradiated for 1 s, scanned again, irradiated for another 1 s, and so on to achieve irradiation times of 1, 2, 3, 4, 5, 10, 20, and 40 s. The reconstructed volumes were subsequently analyzed using DVC using the open-source software Ufreckles developed by J. Réthoré at LaMCoS, INSA de Lyon [21]. In the original developments of DIC and DVC, the registration was performed on zones of interest (ZOIs). These ZOIs are small windows, subset of the considered global and total region of interest (ROI). In these early developments, displacements were assumed to be pure translations [22–27]. In all the cases, of this so called "local approach", the only information kept is the mean displacement of each ZOI. On the contrary, in the approach that we used here, the software performs the registration over the whole region of interest (ROI) at once, no longer divided into subsets. In the literature this is then referred to as a "global approach" [28–35]. It has been shown in [36] that the global approach allows a better measurement resolution and robustness.

For all tests, the samples were kept in the same position, and the µ-CT volumes were reconstructed with the same zone of the detector always selected to ensure that the DVC volume was physically located in the same position inside the sample for each scan. Application of the DVC technique to the same volume before and after polymerization allowed us to determine the displacement and deformation fields caused by shrinkage in the bulk of the composite. Actually, this technique provides the "net displacement", from which we derive the "net strain" (i.e., sum of shrinkage, elastic and creep strain [37,38]). This total "net strain" is what we are looking for as it generates possible incompatibility between the

resin and the tooth, that could subsequently lead to the formation of cracks. From now on, in the rest of the paper, we will then speak about total strain instead of shrinkage strain. The results of the DVC analysis were visualized using the ParaView freeware [39].

To apply the DVC technique, the analyzed volume must be divided into a mesh of finite elements or sub-volumes uniquely identifiable by their grey-level pattern. The DVC software then searches for the position of each element in the initial and final volume (in this case, the volume before and after curing). By comparing these positions, it is possible to calculate the displacement field (with or without rigid body motion) as well as the deformation field from the gradient of the latter. A key parameter is the element size, which must be optimized [40]. Each element must be large enough to be easily (and uniquely) identifiable from one scan to the next. As a rule of thumb, the element size should be at least three times the speckle size. In our case, this rule roughly led to a minimum element size of 21 µm. It has been demonstrated many times [19,41] that a larger element size results in less measurement uncertainty. In contrast, a smaller element size results in higher spatial resolution. The effect of the element size on the uncertainty of the DVC results was assessed by performing a test similar to that reported by Hild *et al.* [41]. An already cured sample was scanned (resolution of 4.5 µm); then, translation along the z-axis was imposed by moving the sample holder, and a second scan was performed. DVC calculations were performed between these two scans. The displacement measurements should be homogeneous within the entire specimen volume. However, in practice, they are not homogenous because of uncertainties arising from the acquisition, reconstruction, and correlation steps of the numerical chain. The standard deviation of this displacement field is typically used as a measure of the cumulated uncertainty, with the total uncertainty calculated as follows [42]:

$$uncertainty = \sigma_{TOT} = \sqrt{\frac{1}{3}(\sigma_x^2 + \sigma_y^2 + \sigma_z^2)}$$

where σ_i is the standard deviation calculated for all the displacements along the *i*-axis in the sample. The standard strain uncertainty is obtained by dividing the movement uncertainty by the element size. To determine the effect of the element size on the uncertainty, the calculations were performed for element sizes of 8, 16, and 32 voxels [41].

Apart from the element size, it should be considered that also other parameters have an influence on the DVC results, such as the speckle density and the overlap between neighboring elements. However, in the present study none of these two parameters could be changed. In fact, since the composite fillers were used as speckles, changing speckle density would require to change the composition of the samples. Moreover, due to the choice of a global approach, each element is linked to the others to assure the continuity of the displacement field, precluding any possible study on the effect of overlapping.

For briefness, the experiments performed on cavities with and without adhesive are referred to as “W” and “WO”, respectively, and those performed without adhesive and in blackened cavities are referred to as “WOb”.

3. Results

3.1 Preliminary tests

The results obtained by subtracting radiographies of uncured samples at different times (data not shown) revealed the following aspects. When an uncured sample was let in the µ-CT chamber with no light nor X-Ray, the upper surface of the specimen moved downwards. This phenomenon was observed also in the other preliminary tests (with natural light and X-Ray irradiation). On the overall, a flow of the upper surface was noticed in the first 50-60 minutes of test. Apart from this flow, no other displacements were noticed when the sample was submitted to continuous X-Ray irradiation nor when it was exposed for 16 hours to the µ-CT chamber light. When, at the end of the experiment, the specimen (after the 16-hour light exposure) was irradiated by the curing unit, the composite shrunk, showing inward movements of all free surfaces of the sample.

3.2. Uncertainty

Figure 1 presents the displacement (and strain) uncertainty (σ_{TOT}) induced by the DVC algorithm. Three different element sizes were analyzed: 32, 16, and 8 voxels. Higher or lower element sizes were excluded because they would likely lead to low spatial accuracy or low precision (high scattering), respectively.

The highest displacement and strain uncertainty (0.8 voxel and 17.7%, respectively) was observed for the smallest element size (8 voxels), whereas the lowest uncertainty (0.1 voxel and 0.5%, respectively) was observed for the largest element size (32 voxels).

3.3. Measurement of polymerization total strain

Figure 2 presents µ-CT images of the same transverse and sagittal sections of the WOb specimen before and after photo-polymerization. After curing, a gap was visible at the interface between the model cavity (in black) and sample (in grey), as observed in the insets of Figure 2B–D. In contrast, no gaps were detected before curing (insert Figure 2C). The dashed lines in Figure 2A–C delimit the volume reconstructed by DVC, which was 600 × 600 × 500 voxels, corresponding to a total volume of 2.7 × 2.7 × 2.3 mm^3, and was meshed into 19 × 19 × 16 elements (hexahedron type) of 32 voxels each to perform the DVC analyses. The edges of the specimens were excluded from the calculation to avoid convergence issues. Nevertheless, to be representative, the analyzed volume included part of the upper surface and part of the core of the specimen (dashed rectangle in Figure 2A). Further studies were performed by selecting a cylindrical volume with the same diameter as the specimen (i.e., approximately 4 mm) and a height of 2.3 mm starting from the upper surface of the sample (dotted lines in Figure 2A–C). The results were scattered because of the presence of the borders of the specimen and are reported only for qualitative evaluations, whereas the quantitative studies were based on the results obtained using the cubic volumes.

The DVC results are presented in Figures 3–5 and reveal the variations between the “uncured” (i.e., before polymerization) and “cured” (i.e., after polymerization) states.

The displacement fields for the three analyzed conditions (W, WO, WOb) are presented in Figure 3. The first three images represent the displacement from which the rigid body motion was subtracted (this is usually named “U”). For this subtraction, the center of the volume is considered a reference point, and the arrows indicate how all the other points of the volume moved compared with this center.

In all three cases, the points of the upper half of the volume moved downward, whereas those of the lower half moved upward. In addition, the arrows in the sample with adhesive (W, Figure 3A) appeared to be mainly aligned along the vertical axis, whereas those in the samples without adhesive (WO and WOb, Figure 3B–C) also displayed a component in the x–y plane.

Figure 3D shows the displacement field, including rigid body motion, of a sample without adhesive. In this case, the reference point was not the center of the analyzed volume (as in Figure 3B) but instead a point external to the volume. The resulting displacement field suggests that the entire volume moved downward and slightly along the x-axis during the polymerization.

The displacement fields (including or not including rigid body motion) were assessed for all the specimens. In particular, the displacement modulus (i.e., the length of the arrow) was calculated for every point (i.e., every subset) of the analyzed volumes. The results are reported in the form of a distribution histogram in Figure 4. The x-axis represents the modulus (in µm) of the displacement without rigid body motion (U), and the y-axis represents the corresponding frequency in the entire volume. Both samples without adhesive exhibited a narrow monomodal distribution of the displacement moduli between 0 and 30 µm. In contrast, the distribution of the displacement moduli in the presence of adhesive appeared broader (extended to between 0 and 50 µm) and ‘bimodal’, with a main peak at 8 µm and a second shoulder at approximately 20 µm.

In addition to the displacement field, the strain field was also assessed by DVC. All 9 components of the strain field were determined for each point of the reconstructed volume; however, for simplicity, only the strains for the main directions (i.e., ε_{xx}, ε_{yy}, ε_{zz}) are reported. We calculated the average and standard deviation of the strain for elements in vertical slices parallel to the top surface of the sample. The average and standard deviation are shown as a function of the depth of the slice in Figure 5. The thickness of a slice corresponds to the thickness of one element, which is 32 voxels, i.e., 144 µm. For each slice, three values are given: ε_{xx}, ε_{yy}, ε_{zz}. Each of these values is the average of all the values of the corresponding strain in the elements of this slice (upper part of Figure 5).

The strain uncertainty is also shown in the graph and, in general, was comparable to (or slightly higher than) the standard deviation of the measured strain.

Comparison of the three analyzed conditions revealed that in all cases, the main strain was along the z-axis. The samples with adhesive displayed the highest values of ε_{zz} (up to –2.5%) but no components on the x- and y-axis. The specimens without adhesive exhibited lower ε_{zz} (on average –1.7% for WO and –1.5% for WOb); however, the strains in the transverse planes were non-negligible. In particular, in the WO samples, the strain was approximately –0.4% in both the x and y directions, and in the WOb specimens, the strain reached –0.5% (both ε_{xx} and ε_{yy}).

In terms of the distribution of the strains within the sample volume, the strains appeared to be quite homogeneous over the entire height of the specimen. Only a slight (not statistically significant) decrease was observed in ε_{zz} at high depths in the WO and WOb specimens.

The inset of Figure 5-WO presents the results obtained for the WO sample when using an element size of 16 voxels (i.e., 72 µm) instead of 32 voxels (as used in all the other calculations). For simplification, only the results between depths of 1152 and 2304 µm are presented in the inset. The strain uncertainty (measured as explained in the Materials and Methods section), also shown in this figure, was higher than that for the 32-voxel element size as well as the standard deviation of the measurement. Logically, when dividing the

element size by two, the number of points in the graph doubled (because each slice was 72-µm high instead of 144-µm high). Overall, the values of strain were unchanged; however, their scattering was greater.

Because the trace of the strain tensor corresponds to the variation in volume $\Delta V/V_0$ (where V_0 is the initial volume), it can be stated that:

$$total\ strain = \frac{\Delta V}{V_0} = \varepsilon_{xx} + \varepsilon_{yy} + \varepsilon_{zz}$$

Using this formula, to calculate the volume total strain of a sample, the average values (calculated over the entire volume of the sample) of ε_{xx}, ε_{yy}, ε_{zz} were summed; the results are reported in Table 1.

For each condition (W, WO, WOb), three different samples were analyzed. The results are reported with the corresponding standard deviation, which indicates the scattering of the total strain values calculated for all the elements in the entire volume of the specimen. All the averages values of total strain are included between 2.0% and 2.6%, and no significant differences were observed between the different samples.

Finally, Figure 6 presents select results obtained from the "interrupted" tests with irradiation times corresponding to 1, 2, 3, 4, 5, 10, 20, and 40 s. Only the strain vs. depth curves for irradiation times of 1, 5, and 40 s are presented for clarity. Non-negligible strains were already observed after 1 s, with a main component along the z-axis (average strain of approximately −1.0%). The modulus of the average value of ε_{zz} tended to decrease (although with no statistical significance) at higher depths. After 5 s of irradiation, all three components of strain still increased, reaching average values of approximately −0.4% for ε_{xx} and ε_{yy} and of −1.3% for ε_{zz}. After 40 s, no further significant evolution of strains was observed, as confirmed by Figure 7, in which the average total strain is shown as a function of irradiation time. The three different curves (black, dark, and light grey) correspond to the results obtained for three different samples, and the error bar represents the standard deviation of total strain inside the volume of a single specimen. For all the samples, the average total

strain rapidly increased in the first 5 s of irradiation from 0.0% to approximately 2.3%–2.4% before reaching a plateau and remaining constant (at approximately 2.4%) until the end of the test.

4. Discussion

4.1 Preliminary tests

The flow of the upper surface observed in all preliminary tests can be attributed to the "packing" of the material induced by gravity (or to surface reactions with atmospheric oxygen) and favored by the change in temperature experienced by the material. Indeed, the composite was stored at ≈4 °C until the beginning of the test, which, on the other hand, was carried out at room temperature. Apart from the upper surface flow, no shrinkage was observed in any of the experiments, confirming that the material did not cure during the test. Indeed, when, at the end of the experiment, the specimen was irradiated by the curing unit, the composite polymerized and shrunk. Therefore, it can be stated that, in the here-analyzed experimental conditions, neither the X-Ray irradiation nor the light of the µ-CT chamber nor the elapsed time caused any relevant shrinkage/curing of the composite. This confirms the validity of the experimental procedure, warning, however, on the need to carry out the experiments on composites already at room temperature (for at least 50 minutes) for avoiding any flow of the upper surface.

4.2 Uncertainty

The results of the current study indicate that a larger element size corresponds to reduced uncertainty, which is consistent with previous findings in the literature [19,41,42]. The results presented in Figure 1 are comparable to those reported in the literature and justify the selection of an element size of 32 voxels. A smaller element size would improve the spatial resolution but would double the displacement uncertainty and increase the strain uncertainty by a factor of 5 (Figure 1). Indeed, as also observed in the inset of Figure 5, upon decreasing the element size from 32 to 16 voxels, the average values of strain remained almost

unchanged; however, the standard deviation dramatically increased. This observation indicates the need to find a good compromise between spatial resolution and scattering of the results, as previously expressed in various reports on digital image correlation [17,40]. When an element size of 32 voxels was used, the strain uncertainty was generally comparable to the scattering of the results (Figure 5). In some cases, however, the strain uncertainty was higher than the standard deviation of the measurements, which implies that small variations of strain in the slice (smaller than the strain uncertainty) will not be detected. Nevertheless, in the present case, an element size of 32 voxels ensured balance between the spatial resolution and scattering; thus, all the results reported in this study were obtained using this element size.

4.3 Measurement of polymerization total strain

As observed in Figure 2, gaps induced by polymerization total strain at the interface between the model cavity and composite were clearly visible in the µ-CT images. DVC analysis was shown to be a powerful tool for quantifying shrinkage and mapping local strains wherever an intrinsic contrast in the microstructure was observed. Indeed, because the filler particles present in the composite were radio-opaque, large enough to be clearly visible by µ-CT, and arranged in a random manner, they fulfilled the function of speckles. Thus, the introduction of additional fillers, which could alter the shrinkage behavior [13–15], could be avoided, and the experimental preparation of the composite was greatly simplified as it could be used as received.

The shrinkage observed in the µ-CT images (insets of Figure 2B–D) was confirmed by the DVC analysis, such as the analysis of the displacement field (without rigid body motion) shown in Figure 3.

In all three cases (Fig. 3A–C), points belonging to both the lower and upper surfaces of the volume moved toward the center of the specimen, confirming the shrinkage of the total volume of the sample. The intensity of the displacement was generally higher for the points

belonging to the upper and lower surfaces, indicating that only shrinkage (and not expansion) occurred inside the volume.

The intensity and direction of the displacement differed from one condition to another, especially for the samples using adhesive (Fig. 3A), for which the arrows were mainly aligned parallel to the z-axis, suggesting that the displacements (and strain) occurred along the height of the specimen. In addition, more dark-red arrows were observed than for the other two samples, indicating that the magnitude of the single displacement was higher. However, in both samples without adhesive (Fig. 3B–C), the arrows also had a component in the x–y plane, indicating that the displacements were not only along the height of the sample but also along its two perpendicular directions. In addition, for both the WO and WOb cases, the intensities of the displacements were comparable. Finally, when the rigid body motion was included (Fig. 3D), all the arrows pointed downward and slightly along the x-axis. This result indicates that while shrinking, the WO sample moved toward the bottom of the cavity and slightly to one side. Because there was no adhesive on the walls, the composite was free to shrink toward the point with the most adhesion, which in this case was most likely located on the bottom-right corner of the cavity. A similar trend was also observed in the WOb samples, whereas in the W samples, the movement was mainly toward the bottom of the cavity without any lateral translation.

Figure 4 confirms the observations on the displacement intensity. When excluding the rigid body motion, the displacements in both samples without adhesive were comparable, whereas those in the sample with adhesive were more scattered with higher values. A similar phenomenon was observed by Chiang *et al.* [14]. This finding can be explained by the fact that when unbonded, the composite can ideally shrink homogeneously in all directions. Therefore, all the displacement vectors have a similar length. However, when some surfaces are bonded, the displacement of the composite is constrained in those directions (inducing only displacements of small magnitude). The unbonded (or weakly bonded) surfaces

compensate for this effect with higher displacements, thereby inducing displacements of higher magnitude.

The differences between the samples were also confirmed by the main strains, which are shown in Figure 5 as a function of the depth in the specimen. In the presence of adhesive, the strain in the x–y plane was close to zero, whereas the strain along the z-axis reached as high as –2.6%. The layer of adhesive strengthens the adhesion between the composite and the lateral wall of the cavity, constraining the contraction of the volume. However, because the upper surface of the restoration is free (as the model cavity is of type 'class I'), the composite can move along the vertical direction (at least, the upper surface can move downwards), which may explain the appearance of the strong strain along the z-axis.

In the absence of adhesive, the composite has no constraints and can shrink in all directions. Indeed, for both the WO and WOb samples, statistically significant components of strain were observed along the x- and y-axis. This finding indicates that the composite also shrunk in the transverse plane, drifting away from the lateral wall of the cavity and inducing the formation of interfacial gaps such as those observed in Fig. 2B–D. In any case, the main component of strain was observed along the vertical axis most likely because the top surface was the only non-constrained surface of the sample and possibly because this surface was in direct contact with the lamp. As previously reported in the literature, shrinkage can be upwards toward the light source, downwards in the opposite direction, or toward the center of mass but always mainly along the axis parallel to the irradiation beam [13–15].

Finally, no significant difference was observed between the WO and WOb specimens, which suggests the limited effect of the transparence of the cavity walls; however, further tests using completely opaque cavities would be necessary to confirm these preliminary results.

Another interesting observation concerns the evolution of the strain ε_{zz} along the depth of the specimen. The intensity of strain tended to decrease in the lower layers of the specimen (i.e., after 1400 µm of depth in Figure 6). This decrease was not statistically significant (because

of the scattering of the data); nevertheless, a similar trend was observed in several tests (Figure 5 and 6). A possible explanation for this phenomenon involves the intensity of the irradiation of the light source, whose evolution follows an exponential law. Accordingly, for a deeper position within the sample, the irradiation of the lamp is weaker; therefore, there is less polymerization (and total strain).

When evaluating the overall strain, it appears that if the total strain is hindered in one direction, this is compensated by more strain in the other directions (as noted in the presence of adhesive). Consequently, regardless of the configuration (i.e., with or without adhesive), the volume total strain was quite similar. As observed in Table 1, the total strain was on average equal to 2.3% (with a minimum of 2.0% and a maximum of 2.6%). Considering the standard deviation of each measurement, no statistically significant differences were observed for the different conditions and samples.

Regarding the evolution of total strain with irradiation time, the results indicate that the main strain occurred in the first 5 s (Figure 7). Indeed, half of the total strain occurred in the first second. Coherent with the observations in the previously described tests, regardless of the irradiation time, the main component of strain was located along the z-axis, with only smaller contributions measured along the x- and y-directions (Figure 6). With increasing irradiation time, all three strain components increased, reaching final values comparable to those obtained in tests performed under similar conditions (i.e., without adhesive, Figure 5). The results of different repetitions (tests 1–3, Figure 7) appear to be homogeneous. The high standard deviation relative to each point can be partially explained by the fact that the average total strain was calculated for the entire specimen volume, even though, as previously demonstrated (Figure 4–5), the strains were observed to be lower in the deeper layers of the sample.

Finally, another interesting question concerns the effectiveness of the “interrupted” tests. Do the kinetics of polymerization stop when the irradiation is interrupted? According to the work of Lecamp *et al.* [43,44], polymerization of non-fully-cured dimethacrylate systems continued

even after the light irradiation stopped. However, this so-called “post-polymerization” is particularly favored at high temperature (higher than the glass transition of the material) and in the absence of oxygen. In the present study, tests were performed at room temperature in the presence of oxygen, two conditions that should hinder post-polymerization. In addition, the results obtained in the interrupted tests (Figure 6) are coherent with those observed when the sample was irradiated continuously for 40 s (Figure 5). Therefore, although the conditions of the “interrupted” tests did not precisely reflect the actual clinical conditions and some post-polymerization could occur, it is here considered that this type of experiments provides useful information (at least qualitative) about the kinetics of total strain. A logical improvement would be to perform ultra-rapid scans while irradiating the composite. This type of test can only be performed in synchrotron facilities, where fast scans (less than 1-s each) and high resolution can be achieved. However, these tests must be carefully planned because the high-energy X-ray beam could induce partial polymerization of the material, compromising the validity of the outcome.

5. Conclusion

In this work, the polymerization-induced strain in dental composite restorations was investigated using model cavities. Different conditions were evaluated, with specific attention paid to the use or absence of adhesive at the interface between the composite and cavity walls. Moreover, the kinetics of total strain was investigated using “interrupted” tests.

As radiopaque fillers were used, the experiments were performed without the need to add other particles, thus avoiding alteration of the shrinkage behavior. µ-CT observations were coupled with DVC analysis (with a global approach) to assess the overall strain as well as the displacement and strain distribution inside the entire specimen. The validity of the DVC results was verified by assessing the effect of certain critical parameters (especially the element size) on the outcome. In addition, preliminary tests were carried out to exclude any possible influence of the experimental procedure (e.g., X-Ray irradiation, ambient light…) on the curing kinetics. On the overall, the results confirm the interest of using DVC for dental

material research, show the effect of a constraint on the shrinkage behavior and provide some guidelines on the choice of DVC parameters and experimental procedure.

In all analyzed cases, the main displacements occurred along the axis parallel to the irradiation beam, inducing preferential strain along the height of the sample (z-axis). In the presence of adhesive, lateral movements were hindered; however, in compensation, vertical movements greater than those measured without the adhesive were observed. No relevant differences were detected when a transparent or blackened cavity was used. However, experiments using a cavity that is completely opaque to light (instead of simply blackened on its external surfaces) would be useful to confirm these observations.

In terms of kinetics, almost all the total strain appeared to occur in the first 5 s of irradiation, suggesting that the usual irradiation time of 40 s applied by dentists should be long enough to avoid any further post-polymerization strain. This finding also confirms the challenge of this study: shrinkage of resin-based composites is so fast that to study this phenomenon, technological facilities and specific experimental set-ups are necessary.

Finally, regardless of the conditions used, the average total strain of the composite was always approximately 2.3%, which suggests that the use of adhesive does not reduce strain but instead limits it to a preferential direction (namely, the one with the highest amount of free surface). This information may be relevant for the practical use of dental composites and lead to new interesting questions concerning the residual stresses inside the material.

As internal residual stresses may be an origin of the degradation of dental restorations, this aspect is worth further investigation; related experiments and simulations are currently being performed by the authors.

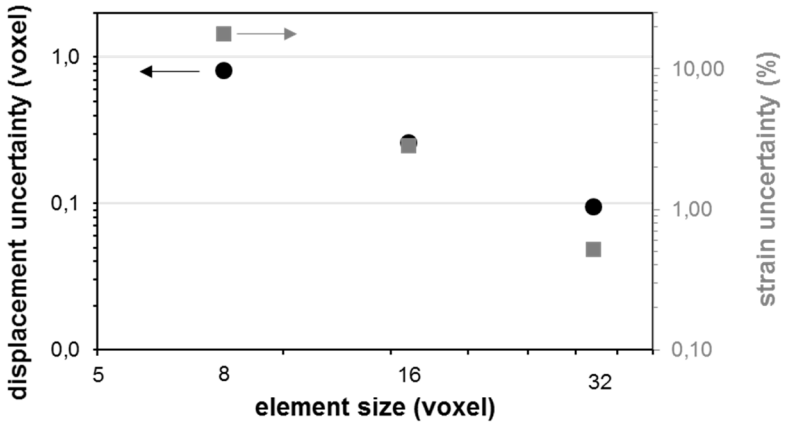

Figure 1

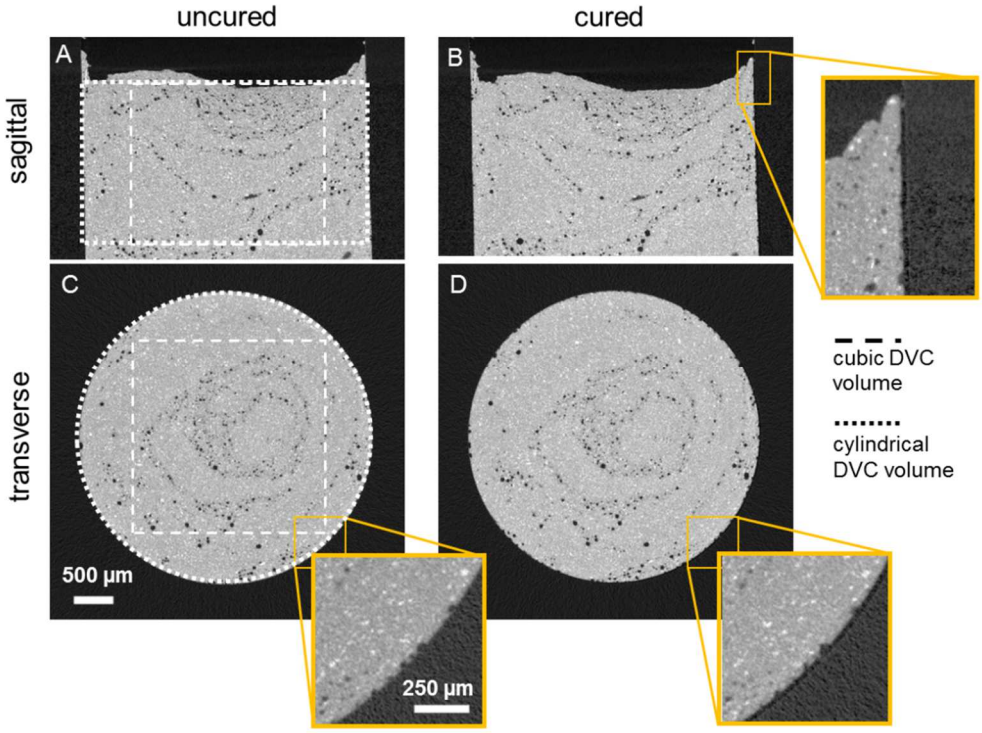

Figure 2

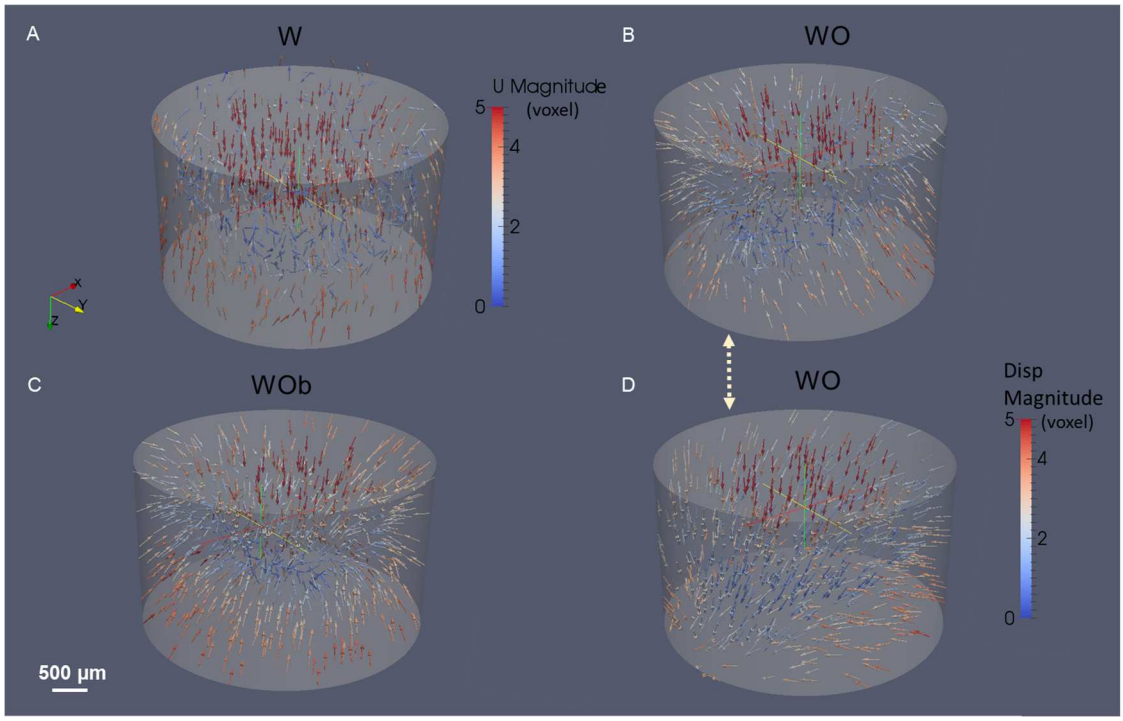

Figure 3

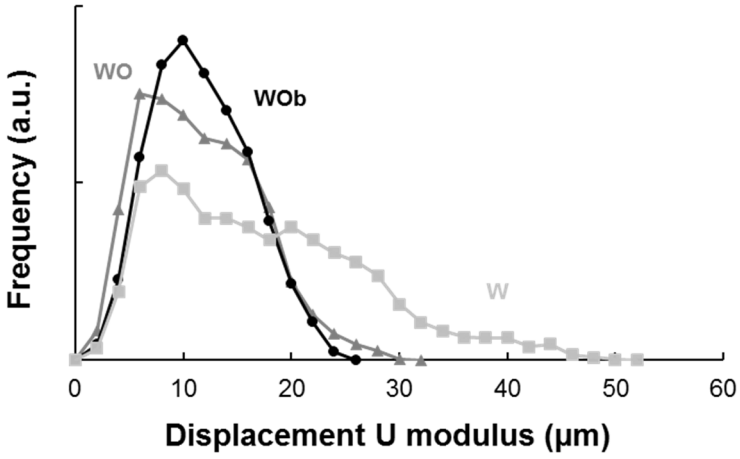

Figure 4

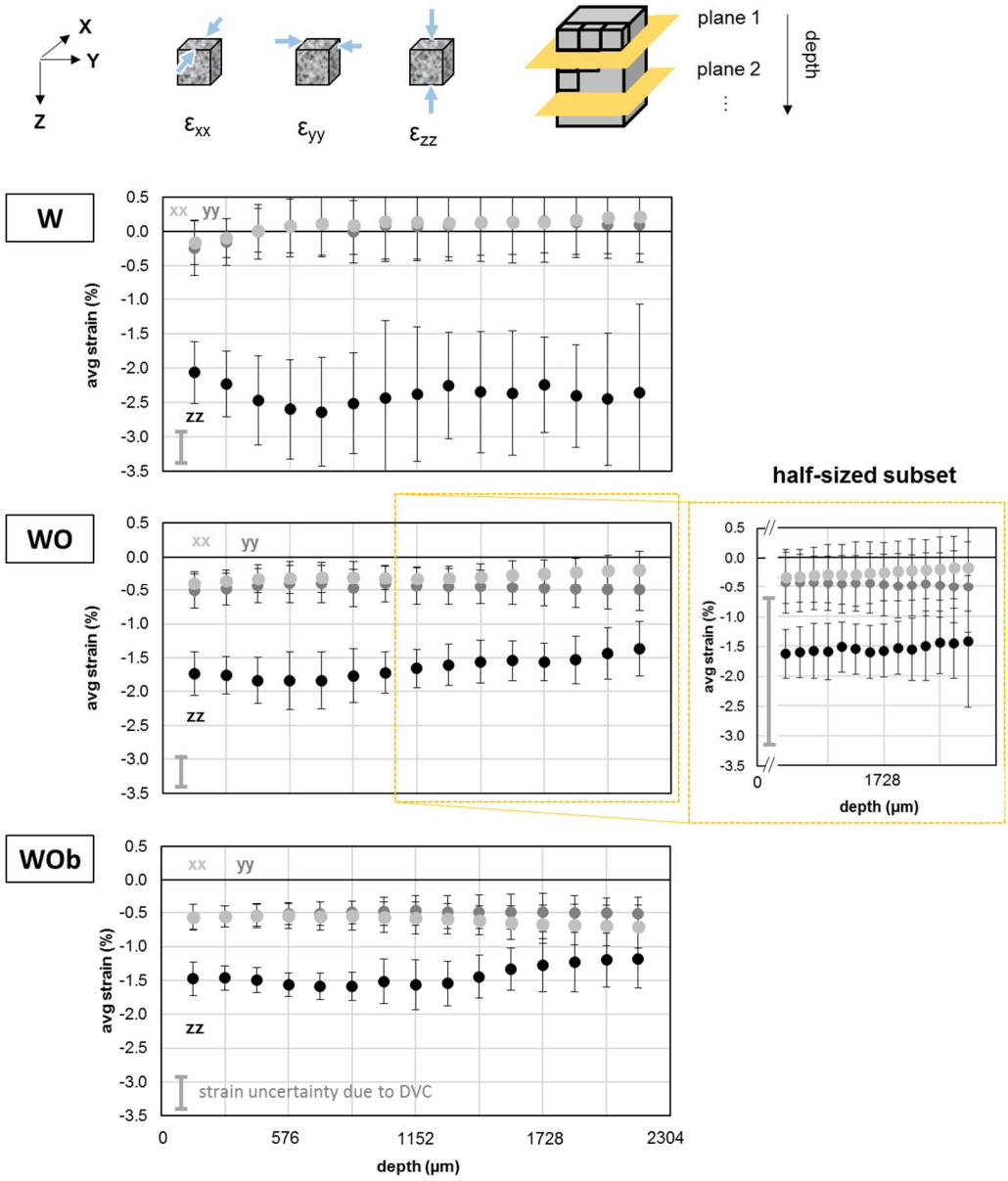
X
Y
Z
εxx
εyy
εzz
plane 1
plane 2
depth
W
WO
WOb
xx
yy
zz
avg strain (%)
half-sized subset
depth (µm)
0
576
1152
1728
2304
strain uncertainty due to DVC

Figure 5

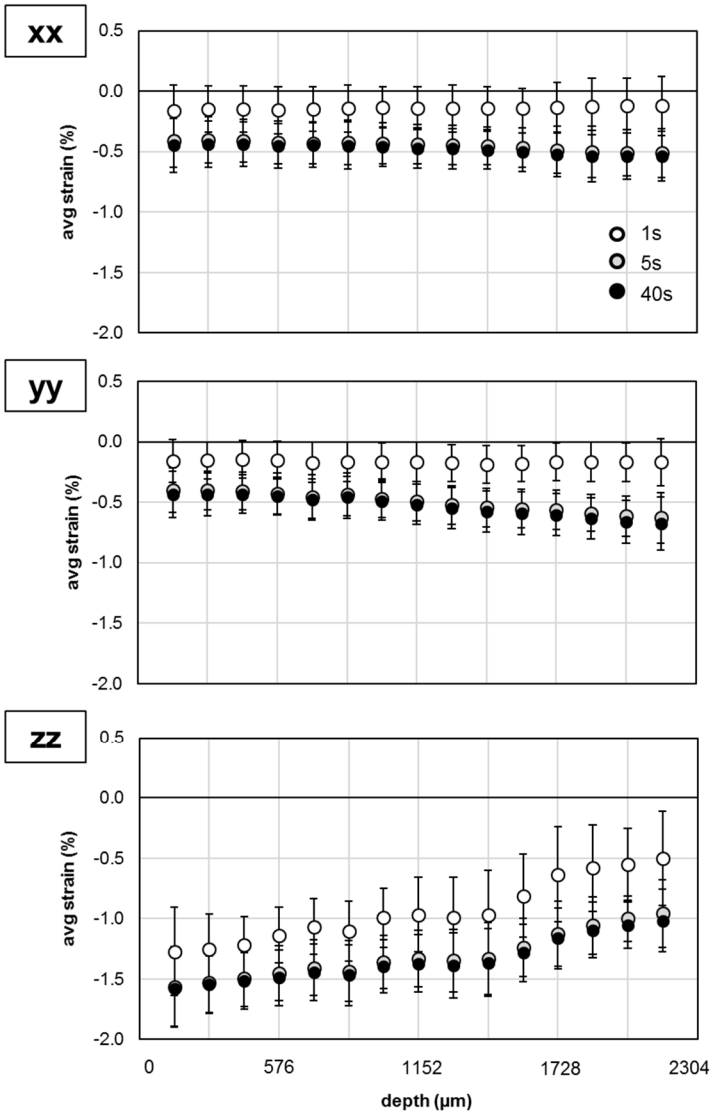

Figure 6

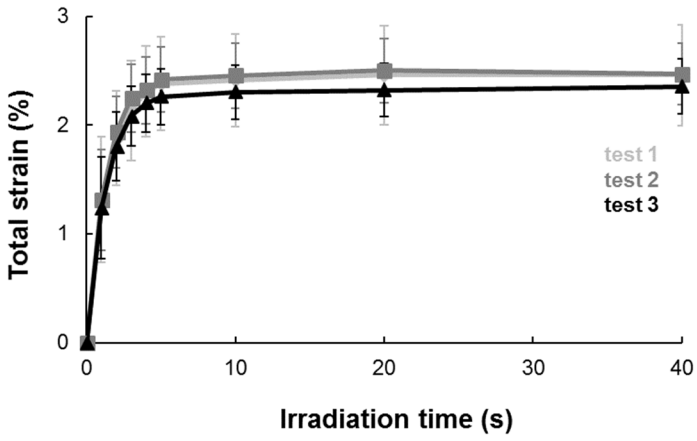

Figure 7

Table 1

	$strain_{avg}$ 1st (%)	$strain_{avg}$ 2nd (%)	$strain_{avg}$ 3rd (%)
W	2.3 ± 1.1	2.0 ± 0.7	2.2 ± 0.5
WO	2.4 ± 0.6	2.4 ± 0.4	2.4 ± 0.4
WOb	2.1 ± 1.1	2.6 ± 0.3	2.5 ± 0.3

Figure Captions

Figure 1: Standard displacement (σTOT) and strain uncertainty as a function of element size when a translation is imposed on the sample (voxel size = 4.5 µm).

Figure 2: Sagittal (A, B) and transverse (C, D) µ-CT images of a sample (without adhesive, blackened cavity) before (A, C) and after (B, D) photo-polymerization. The dashed and dotted lines outline the volume used for DVC.

Figure 3: Displacement field with rigid body motion subtracted ("U") for all three analyzed conditions (A, B, C) and with rigid body motion not subtracted ("Disp") for a sample without adhesive (D) (voxel size = 4.5 µm).

Figure 4: Distribution of the total magnitude of displacements (with rigid body motion subtracted, i.e., U) for the three analyzed conditions.

Figure 5: (Upper part of the figure) Schematic representation of the principal strains and division of analyzed volume into slices and elements. (Lower part of the figure) Distribution of strains (averaged in the different slices) in the three main directions (xx, yy, zz) as a function of the depth of the corresponding slice in the specimen for samples with adhesive (W) and without adhesive (WO and WOb). The inset of figure WO presents the DVC results obtained for the same sample but with a smaller (half) element size. The standard deviation in each plane is given for each measurement. The strain uncertainty for DVC is also indicated in the lower left corner of each graph.

Figure 6: Distribution of strains in the three main directions (xx, yy, zz) as a function of irradiation time and the depth of the corresponding slice in the specimen. The tests were performed in a model cavity without adhesive (WO).

Figure 7: Average total strain as a function of irradiation time. The results were obtained for three different repetitions of samples, all without adhesive.

Table 1: Average values (and corresponding standard deviation) of total strain in the three analyzed configurations (W, WO, WOb). Each test was performed using three repetitions (each one corresponding to a column of the table).

Funding and Acknowledgements

This work was supported by the project TOOTHBOX ANR16-CE08-0024 of the French National Research Agency (ANR).

The authors would also like to thank Nathalie Brulat for demonstrating the experimental procedure for teeth restoration and all the partners of the ToothBox Project for their fruitful discussions and suggestions.

References

[1] Van Nieuwenhuysen J-P, D'Hoore W, Carvalho J, Qvist V. Long-term evaluation of extensive restorations in permanent teeth. J Dent 2003;31:395–405. doi:http://dx.doi.org/10.1016/S0300-5712(03)00084-8.

[2] Demarco FF, Collares K, Coelho-de-Souza FH, Correa MB, Cenci MS, Moraes RR, et al. Anterior composite restorations: A systematic review on long-term survival and reasons for failure. Dent Mater 2015;31:1214–24. doi:https://doi.org/10.1016/j.dental.2015.07.005.

[3] Opdam NJM, van de Sande FH, Bronkhorst E, Cenci MS, Bottenberg P, Pallesen U, et al. Longevity of Posterior Composite Restorations: A Systematic Review and Meta-analysis. J Dent Res 2014;93:943–9. doi:10.1177/0022034514544217.

[4] Ensaff H, O'Doherty DM, Jacobsen PH. Polymerizationshrinkage of dental composite resins. Proc Inst Mech Eng 2001;215:367–75.

[5] Weinmann W, Luchterhandt T, Guggenberger R, Stippschild A, The S, Dede K. Comparative testing of volumetric shrinkage and sealing of silorane and methacrylate filling materials. J Dent Res 2002;81:417.

[6] Burgess J, Cakir D. Comparative Properties of Low-Shrinkage Composite Resins.

Dent Spec Issue 2010;31.

[7] Braga RR, Koplin C, Yamamoto T, Tyler K, Ferracane JL, Swain M V. Composite polymerization stress as a function of specimen configuration assessed by crack analysis and finite element analysis. Dent Mater 2013;29:1026–33. doi:https://doi.org/10.1016/j.dental.2013.07.012.

[8] Carrera CA, Lan C, Escobar-Sanabria D, Li Y, Rudney J, Aparicio C, et al. The use of micro-CT with image segmentation to quantify leakage in dental restorations. Dent Mater 2015;31:382–90. doi:http://dx.doi.org/10.1016/j.dental.2015.01.002.

[9] Neves A, Jaecques S, Van Ende A, Vivan Cardoso M, Coutinho E, Lührs AK, et al. 3D-microleakage assessment of adhesiveinterfaces: Exploratory findings by µCT. Dent Mater 2014;30:799–807.

[10] Jacker-Guhr S, Ibarra G, Oppermann LS, Lührs AK, Rahman A, Geurtsen W. Evaluation of microleakage in class V composite restorations using dye penetration and micro-CT. Clin Oral Invest 2016;20:1709–18.

[11] Sun J, Lin-Gibson S. X-ray microcomputed tomography for measuring polymerization shrinkage of polymeric dental composites. Dent Mater 2008;24:228–34.

[12] Sun J, Eidelman N, Lin-Gibson S. 3D mapping of polymerization shrinkage using X-ray micro-computed tomography to predict microleakage. Dent Mater 2009;25:314–20.

[13] Chiang Y-C, Rösch P, Dabanoglu A, Lin C-P, Hickel R, Kunzelmann K-H. Polymerization composite shrinkage evaluation with 3D deformation analysis from µCT images. Dent Mater 2010;26:223–31. doi:https://doi.org/10.1016/j.dental.2009.09.013.

[14] Chiang Y-C, Hickel R, Lin C-P, Kunzelmann K-H. Shrinkage vector determination of dental composite by µCT images. Compos Sci Technol 2010;70:989–94. doi:https://doi.org/10.1016/j.compscitech.2010.02.017.

[15] Cho E, Sadr A, Inai N, Tagami J. Evaluation of resin composite polymerization by three dimensional micro-CT imaging and nanoindentation. Dent Mater 2011;27:1070–8. doi:http://dx.doi.org/10.1016/j.dental.2011.07.008.

[16] Takemura Y, Hanaoka K, Kawamata R, Sakurai T, Teranaka T. Three-dimensional X-ray micro-computed tomography analysis of polymerization shrinkage vectors in flowable composite. Dent Mater J 2014;33:476–83.

[17] Amini S, Kumar RS. A high-fidelity strain-mapping framework using digital image correlation. Mater Sci Eng A 2014;594:394–403. doi:https://doi.org/10.1016/j.msea.2013.11.020.

[18] Toda H, Maire E, Aoki Y, Kobayashi M. Three-dimensional strain mapping using in situ X-ray synchrotron microtomography. J Strain Anal Eng Des 2011;46:549.

[19] Roux S, Hild F, Viot P, Bernard D. Three dimensional image correlation from X-Ray computed tomography of solid foam. Compos Part A Appl Sci Manuf 2008.

[20] Buffière JY, Maire E, Adrien J, Masse JP, Boller E. In situ experiments with X ray tomography: an attractive tool for experimental mechanics. Exp Mech 2010;50:289–305.

[21] Réthoré J. UFreckles (Version v 2.0). Zenodo. http://doi.org/10.5281/zenodo.1433776 2018.

[22] Lucas BD, Kanade T. An Iterative Image Registration Technique with an Application to Stereo Vision. Proc. 7th Int. Jt. Conf. Artif. Intell. - Vol. 2, San Francisco, CA, USA: Morgan Kaufmann Publishers Inc.; 1981, p. 674–9.

[23] Burt P, Yen C, Xu C. Local correlation measures for motion analysis: a comparative study. Proc. IEEE conf., 1982, p. 269–74.

[24] Sutton MA, Wolters WJ, Peters WH, Ranson WF, McNeill SR. Determination of displacements using an improved digital correlation method. Image Vis Comput

1983;1:133–9. doi:https://doi.org/10.1016/0262-8856(83)90064-1.

[25] Chen DJ, Chiang FP, Tan YS, Don HS. Digital speckle-displacement measurement using a complex spectrum method. Appl Opt 1993;32:1839–49. doi:10.1364/AO.32.001839.

[26] Berthaud Y, Scholz J, Thesing J. Méthodes optiques et acoustiques de mesures des caractéristiques mécaniques. Proc. Colloq. Natl. MECAMAT, 1996, p. 77–80.

[27] F-P Chiang F Lehman, QW. New Developments in Full Field Strain Measurements Using Speckles. Nontradit Methods Sens Stress Strain, Damage Mater Struct n.d.:156–69. doi:10.1520/STP11898S.

[28] Roux S, Hild F, Berthaud Y. Correlation image velocimetry: a spectral approach. Appl Opt 2002;41:108–15. doi:10.1364/AO.41.000108.

[29] Wagne B, Roux S, Hild F. Spectral approach to displacement evaluation from image analysis. Eur Phys J AP 2002;17:247–52.

[30] Cheng P, Sutton MA, Schreier HW, McNeill SR. Full-field speckle pattern image correlation with B-Spline deformation function. Exp Mech 2002;42:344–52. doi:10.1007/BF02410992.

[31] Hild F, Roux S, Gras R, Guerrero N, Marante ME, Flórez-López J. Displacement measurement technique for beam kinematics. Opt Lasers Eng 2009;47:495–503. doi:https://doi.org/10.1016/j.optlaseng.2008.03.006.

[32] Hild F, Roux S. Digital Image Correlation: from Displacement Measurement to Identification of Elastic Properties – a Review. Strain 2006;42:69–80. doi:10.1111/j.1475-1305.2006.00258.x.

[33] Roux S, Hild F. Stress intensity factor measurements from digital image correlation: post-processing and integrated approaches. Int J Fract 2006;140:141–57. doi:10.1007/s10704-006-6631-2.

[34] Leclerc H, Périé J-N, Roux S, Hild F. Integrated Digital Image Correlation for the Identification of Mechanical Properties BT - Computer Vision/Computer Graphics CollaborationTechniques. In: Gagalowicz A, Philips W, editors., Berlin, Heidelberg: Springer Berlin Heidelberg; 2009, p. 161–71.

[35] Réthoré J, Roux S, Hild F. An extended and integrated digital image correlation technique applied to the analysis of fractured samples. Eur J Comput Mech 2009;18:285–306. doi:10.3166/ejcm.18.285-306.

[36] Hild F, Roux S. Comparison of Local and Global Approaches to Digital Image Correlation. Exp Mech 2012;52:1503–19. doi:10.1007/s11340-012-9603-7.

[37] Novaes JB, Talma E, Las Casas EB, Aregawi W, Kolstad LW, Mantell S, et al. Can pulpal floor debonding be detected from occlusal surface displacement in composite restorations? Dent Mater 2018;34:161–9. doi:https://doi.org/10.1016/j.dental.2017.11.019.

[38] Fok ASL, Aregawi WA. The two sides of the C-factor. Dent Mater 2018;34:649–56. doi:https://doi.org/10.1016/j.dental.2018.01.013.

[39] https://www.paraview.org/ n.d.

[40] Rajan VP, Rossol MN, Zok FW. Optimization of Digital Image Correlation for High-Resolution Strain Mapping of Ceramic Composites. Exp Mech 2012;52:1407–21.

[41] Hild F, Maire E, Roux S, Witz J-F. Three-dimensional analysis of a compression test on stone wool. Acta Mater 2009;57:3310–20. doi:https://doi.org/10.1016/j.actamat.2009.03.038.

[42] Lachambre J. Développement d'une Méthode de Caractérisation 3D des Fissures de Fatigue à l'aide de la Corrélation d'Images Numériques obtenues par Tomographie X. Ph.D. thesis. Insa Lyon 2014.

[43] Lecamp L, Youssef B, Bunel C, Lebaudy P. Photoinitiated polymerization of a

dimethacrylate oligomer: 1. Influence of photoinitiator concentration, temperature and light intensity. Polymer (Guildf) 1997;38:6089–96. doi:http://dx.doi.org/10.1016/S0032-3861(97)00184-5.

[44] Lecamp L, Youssef B, Bunel C, Lebaudy P. Photoinitiated polymerization of a dimethacrylate oligomer. Part 3. Postpolymerization study. Polymer (Guildf) 1999;40:6313–20. doi:http://dx.doi.org/10.1016/S0032-3861(99)00042-7.

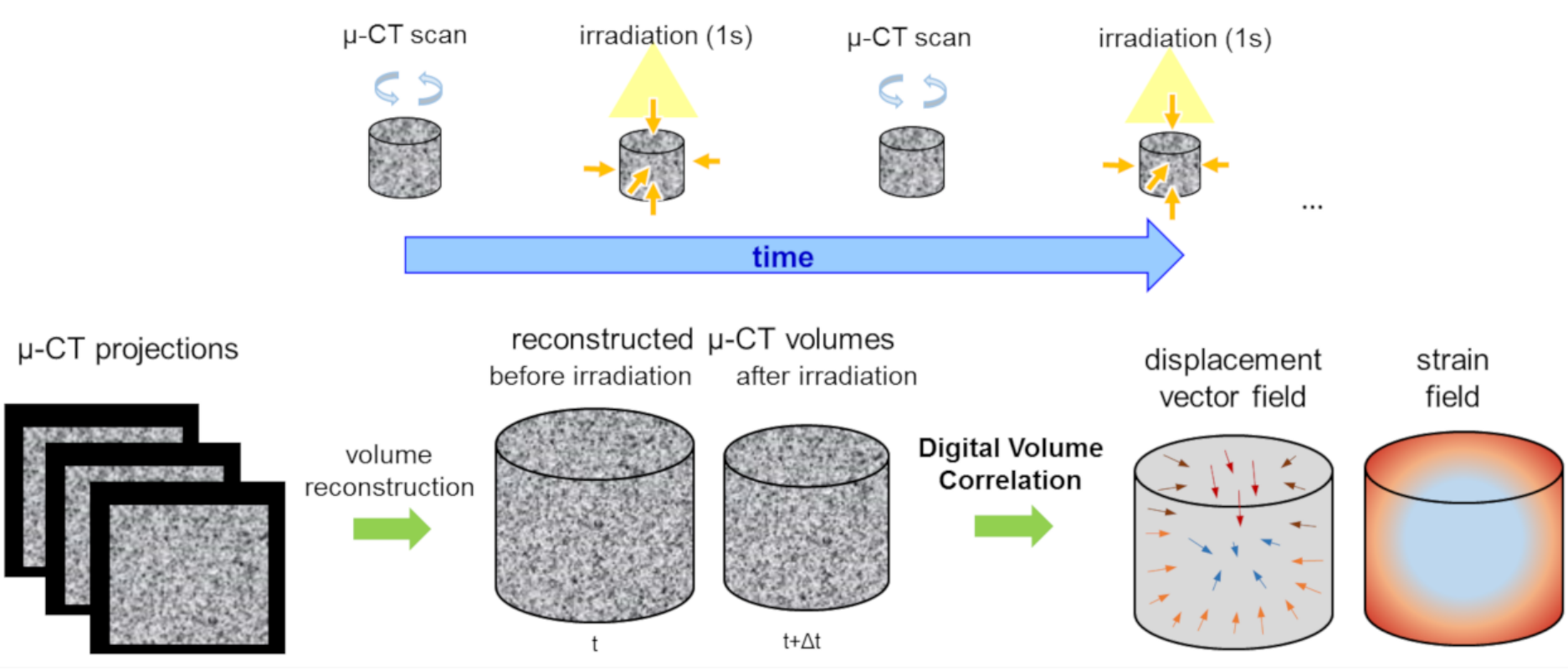
µ-CT scan
irradiation (1s)
µ-CT scan
irradiation (1s)
...
time
µ-CT projections
volume reconstruction
reconstructed µ-CT volumes
before irradiation
after irradiation
t
t+Δt
Digital Volume Correlation
displacement vector field
strain field